ACS Catalysis

Research Article

pubs.acs.org/acscatalysis

Crystal-Plane Effects on the Catalytic Properties of Au/TiO_2

Lichen Liu,[†] Xianrui Gu,[†] Yuan Cao,[†] Xiaojiang Yao,[†] Lei Zhang,[†] Changjin Tang,[†] Fei Gao,*[,‡] and Lin Dong*[,†,‡]

[†]Key Laboratory of Mesoscopic Chemistry of Ministry of Education, School of Chemistry and Chemical Engineering, [‡]Jiangsu Key Laboratory of Vehicle Emissions Control, Center of Modern Analysis Nanjing University, Nanjing 210093, People's Republic of China

Supporting Information

ABSTRACT: In this work, Au nanoparticles are loaded on TiO_2 nanocrystals with different crystal planes exposed ({100}, {101}, and {001} planes) to investigate the crystal-plane effect on the catalytic properties of Au/TiO_2 catalyst. Kinetic studies of CO oxidation show that the catalytic activities of three as-prepared Au/TiO_2 samples follow this order: Au/TiO_2-{100} > Au/TiO_2-{101} > Au/TiO_2-{001}. Furthermore, different mechanisms exist at low temperatures (<320 K) and high temperatures (>320 K). With the help of ex-situ XPS and in situ DRIFTS, the interactions between substrate molecules and different Au/TiO_2 interfaces are investigated. We find that the activation of O_2 and the formation and desorption of carbonates are greatly dependent on the crystal planes of the TiO_2 support. Furthermore, we use CO oxidation as a probe reaction to study the relationships between surface structures and catalytic properties in Au/TiO_2. The catalytic behaviors of three Au/TiO_2 catalysts are well correlated with the spectroscopic results. On the basis of this work, we believe that tuning the crystal plane of TiO_2 support will be an effective strategy to control the catalytic properties of Au/TiO_2.

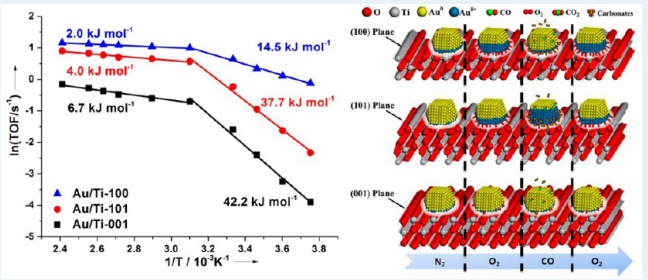

KEYWORDS: *Au/TiO_2, CO oxidation, crystal-plane effect, ex-situ XPS, in situ DRIFTS*

1. INTRODUCTION

Metal nanoparticles (NPs) supported on metal oxides are widely used heterogeneous catalysts with superior activities in many reactions.[1−3] Generally, the metal−oxide interface is the key factor accounting for the catalytic activity and selectivity.[4,5] The size and components of metal NPs are crucial factors that affect the catalytic performance of the metal−oxide interface.[6] Simultaneously, the properties of metal oxide supports also show significant influence.[7,8] However, most of the metal oxide supports in previous works have been in irregular shapes, usually with multiple crystal planes exposed. Considering different surface structures of different crystal planes, the metal−oxide interface may also show crystal-plane-dependent properties.

The crystal-plane effects of metal nanocrystals and metal oxide nanocrystals in catalysis have already been studied in depth.[9] Due to different surface structures and electronic structures, different crystal planes show distinct properties in activation of substrate molecules[10,11] and reaction pathways.[12,13] However, few works are focused on the crystal-plane effect in metal/oxide catalysts. Flytzani-Stephanopoulos et al. have studied the crystal-plane effect on Au/CeO_2 catalysts and have found different abilities of CeO_2 crystal planes in gold stabilization/activation.[14] Yuan et al. have also studied the crystal-plane effect on Au/CeO_2 in the CO-PROX reaction. They proposed that the generation of oxidizing surface H-containing intermediates may be the reason for different activities of Au NPs on different crystal planes of CeO_2,[15] but the metal−support interaction between gold and the different CeO_2 crystal planes and the role of the gold−CeO_2 interface still have not systematically investigated.

In some other works, metal NPs have been loaded onto metal oxides having different crystal planes exposed.[16,17] Although obvious discrepancies of activities are observed, the catalytic results have not been well correlated with their structural differences through spectroscopic characterization. Considering the important role of the metal−oxide interface, it is necessary to study the crystal-plane effect on metal/oxide catalysts on the basis of further analysis and systematic characterization. We should focus on the structural features of different crystal planes in a microscopic view because they are probably the origins of the crystal-plane effects.

Au/TiO_2 and low-temperature CO oxidation over Au/TiO_2 are two of the most typical model catalysts and model reactions that were employed to study the metal−support interaction. On the basis of many intensive studies, the important role of the Au/TiO_2 interface has been recognized.[18−20] The catalytic role of the Au/TiO_2 interface is shown mainly in the absorption

Received: July 1, 2013
Revised: September 26, 2013
Published: October 16, 2013

and activation of substrate molecules (O_2 and CO) at the Au/TiO_2 interface.[21] Herein, through a hydrothermal process, we have prepared anatase TiO_2 nanocrystals with mainly {101}, {100}, and {001} planes exposed. Using these nanocrystals with well-controlled shapes as model supports, we can study the catalytic properties of different Au/TiO_2 interfaces. To the best of our knowledge, this is the first time the catalytic properties of gold NPs supported on different anatase TiO_2 crystal planes have been investigated. Combining the spectroscopic and activity results, we have found that the crystal planes of TiO_2 show significant effects on the catalytic properties of Au/TiO_2.

2. EXPERIMENTS

2.1. Synthesis of TiO_2 Nanocrystals with Different Crystal Planes Exposed. *2.1.1. Synthesis of TiO_2-101. Synthesis of $Ti(OH)_4$ Precursor.* For the preparation of $Ti(OH)_4$, first, an aqueous solution of HCl with a concentration of 0.43 mol/L was prepared, then 6.6 mL of $TiCl_4$ was added to the aqueous HCl dropwise under vigorous stirring in an ice bath to obtain a clear $TiCl_4$ solution. This $TiCl_4$ solution was then added dropwise to a 5.5 wt % aqueous $NH_3{\cdot}H_2O$ solution under stirring. White $Ti(OH)_4$ precipitate was formed during the process. Afterward, about 10 mL of 4 wt % aqueous $NH_3{\cdot}H_2O$ was added to adjust the pH to 6−7. After aging at room temperature for 2 h, the suspension was centrifuged, and the precipitate was washed twice using water two times and once using ethanol. Aqueous $AgNO_3$ (0.05 mol/L) was used to test whether there was residual Cl^- in the supernatant layer. No AgCl was formed after careful washing, suggesting that Cl^- can be fully moved.

Synthesis of TiO_2-101 Nanocrystals. A 2.0 g portion of the fresh $Ti(OH)_4$ precursor and 0.2 g NH_4Cl were dispersed in a mixture of 15 mL of water and 15 mL of isopropyl alcohol. After stirring and ultrasonic treatment, a suspension was obtained. The suspension was then transferred to a 50 mL Teflon-lined autoclave tube and heated for 24 h at 453 K. After the reaction, the products were collected by centrifugation and washed with deionized three times using water and once using ethanol.

2.1.2. Synthesis of TiO_2-100 Nanocrystals. A 0.5 g portion of $(NH_4)_2SO_4$ was dissolved in the mixture of 15 mL of water and 15 mL isopropyl alcohol, then 2.0 g of the fresh $Ti(OH)_4$ precursor was dispersed in the as-prepared mixed solution with the assistance of stirring and ultrasonic treatment. The suspension was then transferred to a 50 mL Teflon-lined autoclave tube and heated for 24 h at 453 K. After the reaction, the products were collected by centrifugation and washed three times using deionized water and once using ethanol. Finally, the product was dried at an oven at 353 K for 6 h. The hydrothermal product was also washed with pure water to remove sulfates tested by a 0.1 mol/L $BaCl_2$ solution.

2.1.3. Synthesis of TiO_2-001 Nanocrystals. TiO_2 nanosheets with {001} planes exposed were prepared by the hydrothermal method reported by Xie et al.[22] In a typical experimental procedure, 25 mL of $Ti(OBu)_4$ (TBOT) and 3 mL of hydrofluoric acid solution (40 wt %) were mixed in a dried Teflon autoclave tube having a capacity of 100 mL and then kept at 453 K for 24 h. After being cooled to room temperature, the white powder was separated by high-speed centrifugation and washed with ethanol and distilled water several times. Finally, these products were dried in an electric oven under air flow at 353 K for 6 h. The hydrothermal product was also washed with 0.1 M NaOH aqueous to remove fluorine. They were then washed with pure water to neutral to obtain surface-clean TiO_2-001 nanocrystals.

2.2. Preparation of Au/TiO_2 Catalysts with Different TiO_2 Crystal Planes Exposed. Au nanoparticles were loaded onto TiO_2 nanocrystals having different crystal planes exposed through deposition−precipitation. The loading amount of Au is 2 wt %. A 1 g portion of TiO_2 nanocrystals was put in a mixture of aqueous $HAuCl_4$ (0.0243 mol/L, 4.18 mL) and 0.605 g of urea. This mixture was stirred at 353 K for 16 h, then the suspension is centrifuged at 8000 rpm and washed with aqueous NaOH (0.1 mol/L). Afterward, the product was washed three times using water to neutral before it was dried at 353 K. Finally, the product was calcined at 573 K for 2 h in air.

2.3. Characterization. X-ray diffraction (XRD) measurement patterns were recorded on a Philips X'pert Pro diffractometer using Ni-filtered Cu Kα1 radiation (λ = 0.15 nm). The X-ray tube was operated at 40 kV and 40 mA.

Transmission electron microscopy (TEM) images were taken on a JEM-2100 instrument at an acceleration voltage of 200 kV. The samples were crushed and dispersed in A.R. grade ethanol, and the resulting suspensions were allowed to dry on carbon film supported on copper grids.

In-situ ESR signals of O_2^- were recorded at ambient temperature on a Bruker ESR A200 spectrometer. After bubbling O_2 for 10 min at 303 K, the Au/TiO_2 catalysts were introduced into the homemade quartz cup inside the microwave cavity and kept in N_2 atmosphere for ESR characterization to exclude the influence of O_2. The settings for the ESR spectrometer were as follows: center field, 3233.0 G; sweep width, 100 G; microwave frequency, 9.055 GHz; modulation frequency, 200 kHz; power, 10.00 mW. Magnetic parameters of the radicals detected were obtained from direct measurements of magnetic field and microwave frequency.

Ex-situ X-ray photoelectron spectroscopy (XPS) analysis was performed on a PHI 5000 VersaProbe system using monochromatic Al Kα radiation (1486.6 eV) operating at 25 W. The sample was outgassed overnight at room temperature in a UHV chamber ($<5 \times 10^{-7}$ Pa). All binding energies (BE) were referenced to the C 1s peak at 284.6 eV. The experimental errors were within ±0.1 eV. During the ex-situ XPS experiments, the samples were first pretreated in the corresponding atmosphere for 1 h, then the sample was sent to the UHV chamber for XPS testing. After collecting XPS signals, the samples were sent to the reaction chamber again for pretreatment in another atmosphere.

In-situ DRIFT spectra were collected from 400 to 4000 cm^{-1} at a spectral resolution of 4 cm^{-1} (number of scans, 32) on a Nicolet 5700 FT-IR spectrometer equipped with a DTGS as the detector. The sample was pressed into a self-supporting wafer (about 15 mg) and mounted in a commercial controlled environment chamber (HTC-3). The wafer was pretreated with high-purity N_2 at 473 K for 1 h. After cooling to ambient temperature, the sample was exposed to a controlled stream of CO−Ar (10% of CO by volume) at a rate of 5.0 mL min^{-1} for 45 min for saturation. The desorption studies were performed under a controlled stream of O_2−Ar (5% of O_2 by volume) at a rate of 5.0 mL min^{-1}.

2.4. Catalytic Activity Measurement. The CO oxidation activities of Au/TiO_2 catalysts were measured in a flow microreactor with a gas composition of 1.6 vol % CO, 1.6 vol % O_2, and 96.8 vol % N_2 at a space velocity of 300 000 mL g^{-1} h^{-1}, and 50 mg catalyst was used for each measurement. The

dx.doi.org/10.1021/cs400492w | ACS Catal. 2013, 3, 2768−2775

catalyst was pretreated in a N_2 stream at 473 K for 1 h and then cooled to room temperature. After that, the mixed gases were switched on. Two columns and a thermal conductivity detector (TCD) were used for the purpose of analyzing the production, column A with 13× molecular sieve for separating O_2, N_2 and CO, and column B, packed with Porapak Q for separating CO_2.

In the kinetic study, only 5 mg of catalyst was used to keep the conversion of CO below 20%. The kinetic study was carried out in sequential measurements as a function of the reaction temperature.

In the catalytic measurements of CO-PROX, a gas mixture ($CO/O_2/H_2/He$ = 1:1:49:49 by molar ratios) was fed with GHSV = 30 000 h^{-1}. A limited amount of oxygen (O_2/CO molar ratio = 1) was used in this study. Because the difference in H_2 concentration on stream was very small and was difficult to analyze by gas chromatography, CO and O_2 concentrations were analyzed and used to calculate CO conversion and selectivity of O_2 reacting with CO, which was defined as CO selectivity. The CO conversion and CO selectivity were calculated using the following equations:

$$\text{CO conversion} = \{[\text{CO}]_{\text{in}} - [\text{CO}]_{\text{out}}\}/[\text{CO}]_{\text{in}} \quad (1)$$

$$\text{CO selectivity} = 0.5 \times \{[\text{CO}]_{\text{in}} - [\text{CO}]_{\text{out}}\} / \{[\text{O}_2]_{\text{in}} - [\text{O}_2]_{\text{out}}\} \quad (2)$$

3. RESULTS AND DISCUSSIONS

Through introducing different anions, growth directions of TiO_2 nanocrystals can be controlled during hydrothermal processes (as described in Section 2.1). XRD patterns of these TiO_2 nanocrystals are shown in Supporting Information (SI) Figure S1. All three samples show the typical diffraction patterns of anatase TiO_2. XRF and XPS results (not shown here) confirm that the anions used in the synthesis have been fully removed by washing with NaOH aqueous. The TEM images of anatase TiO_2 nanocrystals with different crystal planes ({101}, {100}, and {001}) exposed are shown in SI Figure S2. On the basis of the Wulff construction (SI Figures S3−S5), we can calculate the proportions of each crystal plane in these samples (SI Table S1). As we can see, the proportion of each crystal plane is above 80%, indicating that these TiO_2 nanocrystals can be used as model supports. From SI Figures S3−S5, we can also see that the average sizes of TiO_2 nanocrystals range from 50 to 70 nm; therefore, the nanosized effect of the TiO_2 nanocrystals should not be the factor affecting the catalytic properties in this work.

Au/TiO_2 catalysts are prepared through the classic deposition-precipitation (DP) method. XRD results (SI Figure S6) show that the anatase-type crystal forms of the TiO_2 supports are preserved after Au loading. Transmission electron microscopy (TEM) is used to figure out the morphologies of Au/TiO_2 catalysts and the location of Au NPs. As presented in Figure 1, the shapes of TiO_2 nanocrystals with different planes exposed are preserved after Au loading, without aggregation or distortion. HRTEM images show that hemispherical Au NPs are anchored on {101}, {001}, and {100} planes of anatase TiO_2 nanocrystals, indicating the interaction between Au NPs and different TiO_2 crystal planes. Because the DP conditions (base, pH value, time, calcination temperature, etc.) are strictly controlled, the average sizes of gold NPs in these three samples are quite close, ~3.6 nm (size distributions of Au NPs are shown in SI Figure S7). From SI Table S2, we can find that the

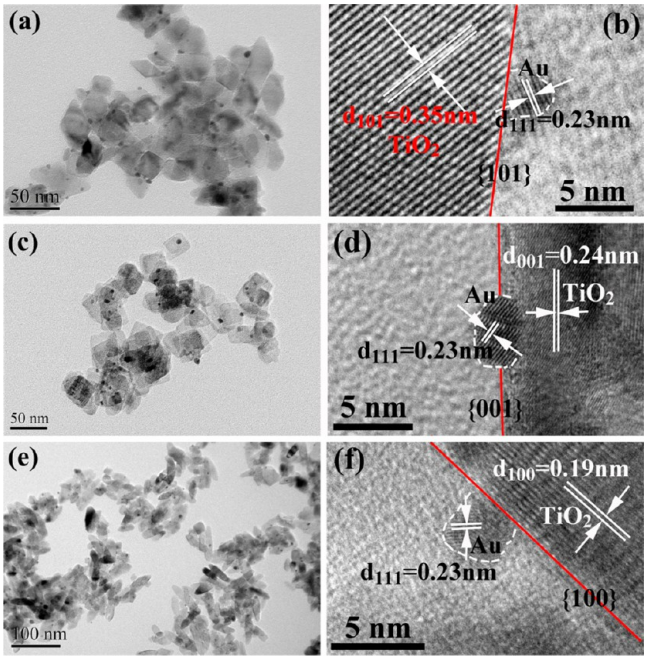

Figure 1. TEM images of Au/TiO_2 catalysts with different TiO_2 crystal planes. (a, b) Au/Ti-101, (c, d) Au/Ti-001, and (e, f) Au/Ti-100.

surface areas are quite close for three Au/TiO_2 catalysts. On the basis of the above analysis, we can conclude that the as-prepared Au/TiO_2 catalysts with different TiO_2 crystal planes exposed are ideal model catalysts to study the crystal-plane effect on the catalytic properties.

Low-temperature CO oxidation is used as the model reaction, and the raw activity curves are presented in SI Figure S8. The Au/Ti-100 sample shows the best activity: 100% CO conversion at 253 K. As for Au/Ti-101 and Au/Ti-001, 100% CO conversion has been achieved at 273 and 303 K, respectively. Furthermore, Arrhenius plots of Au/TiO_2 catalysts are shown in Figure 2. In the calculation of TOF, only the gold atoms located at the perimeters of Au/TiO_2 interfaces are counted.[23] Obviously, the Au/Ti-100 shows the highest TOF in CO oxidation, and the Au/Ti-001 shows the lowest TOF. Interestingly, above 320 K, the values of E_a (apparent activation energy) are quite low for these three samples; however, below

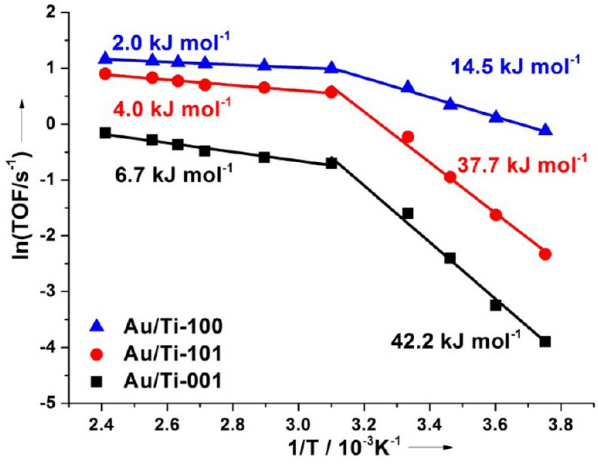

Figure 2. Kinetic studies of CO oxidation reaction on Au/TiO_2 catalysts with different TiO_2 crystal planes.

dx.doi.org/10.1021/cs400492w | ACS Catal. 2013, 3, 2768−2775

320 K, the values of E_a become much larger, and the discrepancies among the three samples are obvious. These results are similar to some previous works.[20−25]

Haruta et al. proposed that there may be two mechanisms: at low temperature (<320 K), and at relatively high temperature (>320 K).[20] Fujitani et al. demonstrated that at low temperature, O_2 would first react with H_2O to form hydroperoxides and then react with CO to form CO_2. This process occurs at the Au/TiO_2 interface, whereas at higher temperature, O_2 is activated by low-coordinated Au atoms and reacts with CO on the Au NPs.[24] However, in the work of Behm et al., they proposed that the atomic oxygen species should be the active species when the temperature is above 350 K, and the atomic oxygen species can migrate to the Au/TiO_2 interface to oxidize CO to CO_2.[25] Despite the differences in those works, they all demonstrated that O_2 is activated at the Au/TiO_2 interface at low temperature (<320 K) and different mechanisms may exist at different temperaturs in CO oxidation.

In this work, the Au NPs are supported on different TiO_2 crystal planes, forming different Au/TiO_2 interfaces. The O_2 activation at the interface will be affected by the different atomic structures of different TiO_2 crystal planes, leading to discrepancies in apparent activation energy. Previous works show that O_2 is usually activated through getting one electron to form O_2^-.[26] To measure their abilities of different Au/TiO_2 interfaces in O_2 activation, we have carried out an in situ ESR experiment. After O_2 pretreatment on these samples at 303 K, we collected the ESR signals as shown in SI Figure S9. The signals located at g = 2.001, 2.006, and 2.024 can be ascribed to the superoxide ions (O_2^-).[27] Obviously, the O_2^- signal is much stronger in Au/Ti-100 than in Au/Ti-101 and Au/Ti-001, indicating that more O_2^- species are formed on the surface in Au/Ti-100. Combining the in situ ESR and CO oxidation activity results, we can see that Au/Ti-100 is active in O_2 activation at low temperature, whereas Au/Ti-001 is inert. According to previous studies, surface hydroxyl groups play a crucial role in O_2 activation on Au/TiO_2.[28]

For anatase TiO_2 nanocrystals, the amounts of hydroxyl groups will vary with the crystal planes as a result of the different surface structures.[29] The amounts of surface hydroxyl groups in the three Au/TiO_2 catalysts were measured by XPS. As shown in Figure 3, the peaks located at 529.72 and 531.60 eV can be ascribed to lattice oxygen (O−Ti) and the surface hydroxyl group (O−H), respectively. The amounts of surface hydroxyl groups can be estimated through calculating the ratio of the areas of O−H and O−Ti.[30] According to the results in Table 1, the order of amounts of surface hydroxyl groups is Au/Ti-100 > Au/Ti-101 > Au/Ti-001, which is consistent with their catalytic activities. These results suggest the surface structures of different TiO_2 crystal planes can exhibit significant influences on Au/TiO_2 catalysts in activating substrate molecules.

In addition, the crystal-plane effects may also affect the catalytic properties of Au/TiO_2 catalysts in selective oxidation reactions for their quite different performances in O_2 activation. Herein, we choose CO preferential oxidation in rich H_2 (CO-PROX) to test their selectivity. As displayed in SI Figure S10, the Au/Ti-100 shows better CO conversion than Au/Ti-101 and Au/Ti-001, especially at low temperature (<320 K). Because O_2 activation is the crucial step in many oxidation reactions catalyzed by supported Au NPs,[1] controlling the crystal planes of the supports may be one strategy to obtain the desired activity and selectivity.

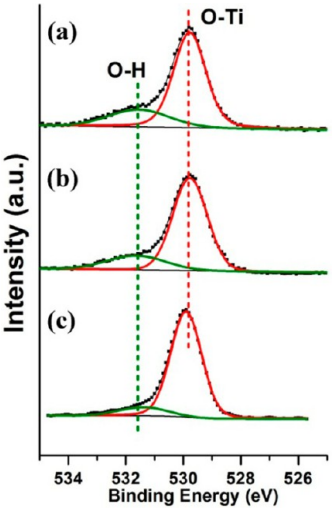

Figure 3. O 1s region of XPS spectra of (a) Au/Ti-100, (b) Au/Ti-101, (c) and Au/Ti-001.

Table 1. XPS Peak Information of O 1s Region after Fitting

	Ti−O		O−H		O−H/O−Ti
	binding energy/eV	area/ a.u.	binding energy/eV	area/ a.u.	
Au/Ti-100	529.72	8125	531.60	2898	0.36
Au/Ti-101	529.73	7789	531.61	2125	0.27
Au/Ti-001	529.72	7856	531.60	865	0.11

In Figure 2, at higher temperature (>350 K), the values of apparent activation energy (E_a) for three Au/TiO_2 catalysts become much smaller and quite close to each other. Because the activation of O_2 will be easier to achieve at high temperature, the apparent activation energy becomes much smaller.[31] Moreover, activated lattice oxygen species at the perimeter of the Au/TiO_2 interface are the main active species.[25] The migration of lattice oxygen depends on the surface structure of the TiO_2 support. As shown in SI Figure S11, the atomic structures of {100}, {101}, and {001} facets are different from each other. The coordination environment of oxygen and titanium will show significant influences on the dissociation of O_2 and migration of oxygen. The oxygen migration behavior on {100} and {101} planes may be more facilitated than on {001} planes, resulting in their higher activities at >350 K.[32]

The activation of O_2 should have great influence on the chemical states of Au, so we used ex-situ XPS spectra to investigate the interactions between Au/TiO_2 and the substrate molecules (O_2 and CO). In the ex-situ XPS characterizations, the samples were pretreated in a sequence of different atmospheres to study the chemical states of Au in different environments. The XPS spectra of the Au 4f region are presented in SI Figure S12 and Figure S13. As we know, positive Au species (Au^+ and Au^{3+}; they are denoted as $Au^{\delta+}$) may contribute to the high activity in the CO oxidation.[33,34] After fitting these spectra, the amounts of $Au^{\delta+}$ are calculated and shown in Figure 4. Let us discuss the data obtained at low temperature (303 K) first (in Figure 4a). After using N_2 pretreatment to clean the surface, three Au/TiO_2 catalysts show a relatively low content of positive Au species. To observe the dynamic changes of the surface properties of gold NPs, the Au/TiO_2 catalysts were treated, in turn, in CO and O_2

dx.doi.org/10.1021/cs400492w | ACS Catal. 2013, 3, 2768−2775

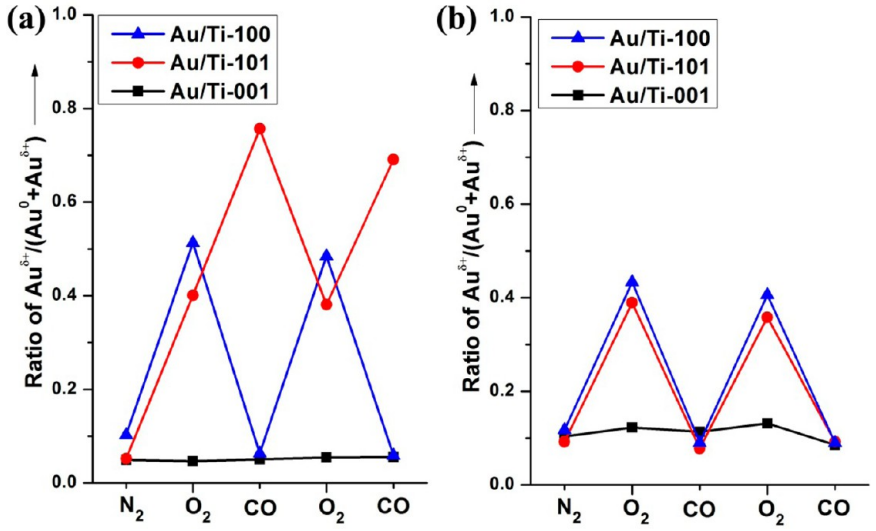

Figure 4. Ratio of $Au^{\delta+}/(Au^0 + Au^{\delta+})$ calculated from the ex-situ XPS spectra in different Au/TiO_2 catalysts at (a) 303 K and (b) 353 K in a sequence of different atmospheres.

atmospheres. After O_2 treatment for 1 h, the content of the $Au^{\delta+}$ increased to 45% and 35% in Au/Ti-100 and Au/Ti-101, respectively. This increase may be caused by the absorption of oxygen species on the surface of the Au/TiO_2 and oxidation of Au to higher chemical states;[35,36] however, the content of $Au^{\delta+}$ in Au/Ti-001 remains almost stable.

These samples were then treated with CO for 1 h, and the $Au^{\delta+}$ contents show quite a distinct tendency in different samples. The Au/Ti-001 remains unchanged, indicating that the Au NPs supported on the {001} planes of the anatase are inert to the switches of atmosphere. As for the $Au^{\delta+}$ in the Au/Ti-100, the content goes down to 12% as a result of the reduction of $Au^{\delta+}$ to Au^0. Interestingly, the $Au^{\delta+}$ content in the Au/Ti-101 continues to increase after CO treatment. When we switched to the O_2 treatment, the $Au^{\delta+}$ content in Au/Ti-100 and Au/Ti-101 reverted to around 40%, which was similar to the first O_2 treatment process. When they were treated with CO again, the $Au^{\delta+}$ in the Au/Ti-101 jumped to the higher content again, and the $Au^{\delta+}$ in the Au/Ti-100 fell back to a low content. Thus, a chemical oscillation in Au/Ti-100 and Au/Ti-101 can be observed during the ex-situ XPS experiments. For the Au/Ti-001 sample, the chemical states of Au are insensitive to the atmosphere, inferring the inert properties of Au NPs supported on {001} planes. This could account for the poor activity of Au/Ti-001 in CO oxidation. Although Au/Ti-100 and Au/Ti-101 show different changes under CO and O_2 atmosphere, their chemical states are both quite sensitive to the atmosphere. Because of the flexible changes in the chemical states of gold during alternate treatments of O_2 and CO, the Au/Ti-100 and Au/Ti-101 show a much better activity in CO oxidation than does Au/Ti-001.[37] The different variation tendencies of Au in Au/Ti-100 and Au/Ti-101 will be discussed below.

When the temperature increased to 353 K, the chemical oscillations of Au species also appeared in three samples (Figure 4b); however, the variation tendencies of the $Au^{\delta+}$ content under different atmospheres are different from those at 303 K. At 353 K, Au/Ti-001 shows a slight oscillation driven by CO and O_2, which is consistent with its higher activity above 320 K. Au/Ti-100 has almost the same variation tendency as those at 303 K, whereas Au/Ti-101 has a tendency similar to Au/Ti-100. Because of the thermal desorption of the oxygen species at higher temperature, the percentages of $Au^{\delta+}$ in Au/Ti-101 and Au/Ti-100 at 353 K are slightly lower than those at 303 K.[38] Combining the activity results and XPS analysis, they further confirm that different mechanisms should exist at different temperatures.

Because the formation of carbonates and other related species are crucial steps during CO oxidation, in situ DRIFTS was performed to study the catalytic mechanisms on different Au/TiO_2 catalysts at 303 K (shown in Figure 5). Herein, to observe the formation process of carbonates and other related species, Au/TiO_2 catalysts were first pretreated with O_2. No significant changes in the DRIFTS, as compared with those obtained under N_2 atmosphere, were observed. The atmosphere was then shifted to CO, leading to the formation of carbonates as shown in Figure 5a, c, and e. The peak intensities at 1600−1200 cm^{-1} gradually increased with time. Notably, the amounts of carbonates in Au/Ti-001 are much smaller than those on Au/Ti-101 and Au/Ti-100, which may be a result of its low activity in O_2 activation. Interestingly, the kinds of carbonates formed on the three Au/TiO_2 catalysts are also different. Only bidentate carbonate (b-CO_3^{2-}, at 1308 and 1555 cm^{-1}) and bicarbonate (HCO_3^-, at 1405−1425 cm^{-1} and 1626 cm^{-1}) are formed on Au/Ti-001. Peaks corresponding to monodentate carbonate (m-CO_3^{2-}, at 1512 and 1364−1384 cm^{-1}) and solvated carbonate (s-CO_3^{2-}, at 1321−1323 cm^{-1}) can be observed in Au/Ti-100 and Au/Ti-101.[39−41] A small amount of bicarbonate can also be observed in Au/Ti-101. Because Au/Ti-101 and Au/Ti-100 are much more active than Au/Ti-001 in CO oxidation, the m-CO_3^{2-} and s-CO_3^{2-} are important intermediate products during CO oxidation, which has been predicted by experimental theoretical calculations.[42,43] s-CO_3^{2-} species are usually formed through the reaction of surface hydroxyl groups (located at the Au/TiO_2 interface) and CO.[44] According to XPS analysis, there are more surface hydroxyl groups on the {100} plane and the {101} plane, resulting in formation of s-CO_3^{2-} on Au/Ti-100 and Au/Ti-101. Because of the different atomic structures ofthe Au/TiO_2 interfaces in the three Au/TiO_2 catalysts, the formation of m-CO_3^{2-} may be facilitated in $Au/TiO_2(101)$ and $Au/TiO_2(100)$ interfaces, leading to their higher activities. On the basis of the

dx.doi.org/10.1021/cs400492w | ACS Catal. 2013, 3, 2768−2775

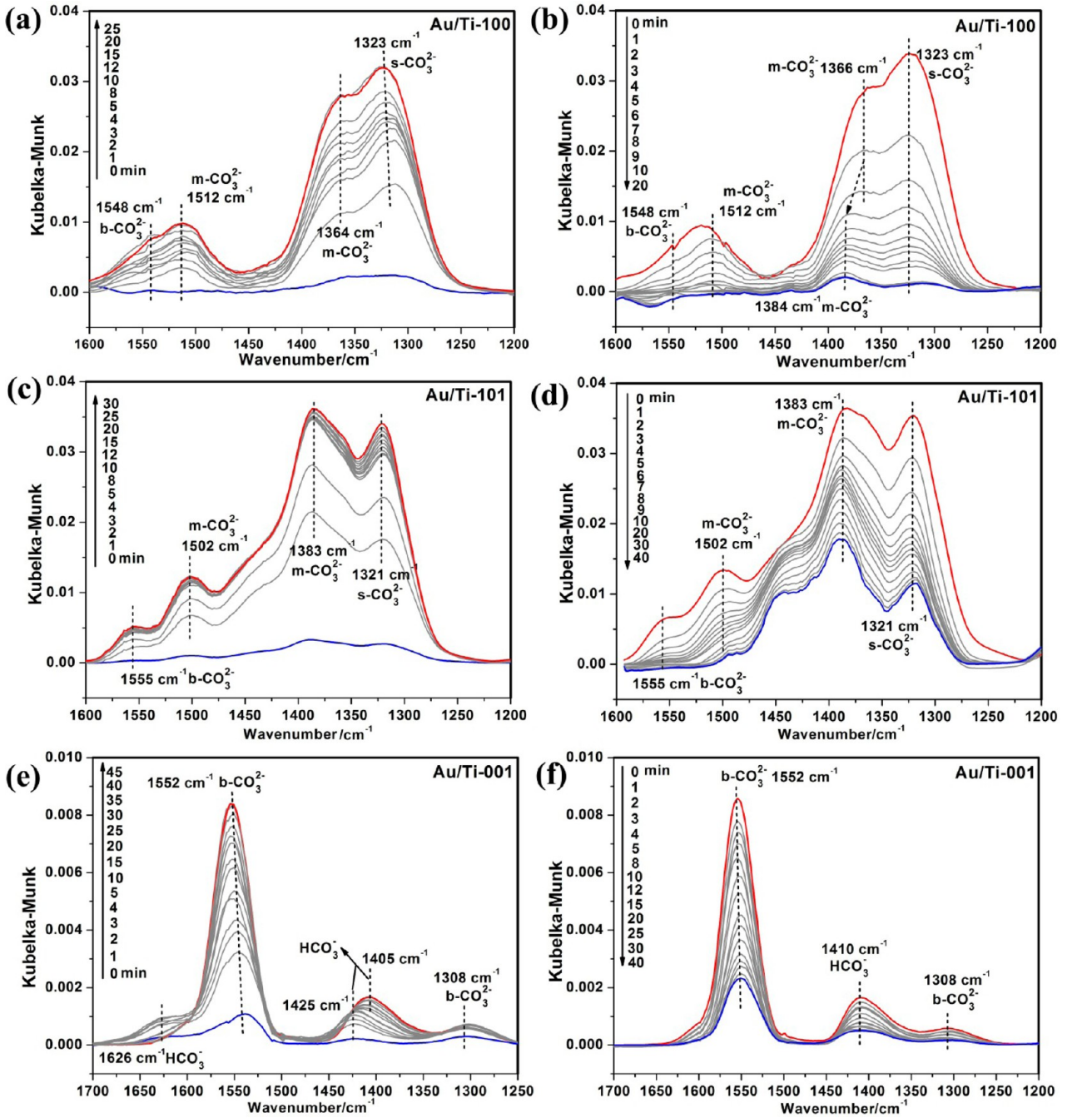

Figure 5. In-situ DRIFTS of the carbonates on Au/TiO_2 catalysts at 303 K. The Au/TiO_2 samples were first pretreated in O_2 for 1 h, then the atmosphere was shifted to CO. (a, c, e) Data collected in CO atmosphere. After pumping CO for 1 h, the atmosphere is shifted to O_2. (b, d, f) Data collected in O_2 atmosphere.

identification of carbonates, CO oxidation may follow different mechanisms on active Au/Ti-100 and Au/Ti-101 and on inactive Au/Ti-001.

The formation rates of carbonates also need to be noted, especially, the amounts of carbonates that are close to saturation after CO absorption for only 4 min in Au/Ti-101, whereas, it takes ~20 min or more to achieve saturated absorption in Au/Ti-100 and Au/Ti-001. The vibration properties of carbonates that absorbed on Au/TiO_2 catalysts are also affected by the crystal plane of the TiO_2 support. In the Au/Ti-101 sample, the peak corresponding to m-CO_3^{2-} is located at 1383 cm^{-1}, whereas that peak is located at 1364 cm^{-1} in the Au/Ti-100 sample. We have tested the in situ DRIFTS of pure TiO_2 support under similar conditions (SI Figure S14). Through comparing the spectra of Au/Ti-100 and TiO_2-100, the m-CO_3^{2-} with lower vibrational energy can be ascribed to carbonates absorbed on the TiO_2 support. According to the literatures, the m-CO_3^{2-} species at 1383 cm^{-1} can be ascribed to carbonates absorbed on Au NPs;[45,46] therefore, the distributions of m-CO_3^{2-} in Au/Ti-100 and Au/Ti-101 are different. In Au/Ti-101, carbonates generate mainly at the Au/TiO_2 interface, and they show strong binding interaction with Au NPs. As for Au/Ti-100, carbonates will move to the TiO_2 support after formation at the Au/TiO_2 interface. Because of

dx.doi.org/10.1021/cs400492w | ACS Catal. 2013, 3, 2768−2775

the strong interaction between Au NP and m-CO_3^{2-} in Au/Ti-101, electrons will transfer from the Au NP to m-CO_3^{2-}, resulting in the further increase of the $Au^{\delta+}$ content in the Au/Ti-101 sample after CO treatment during the ex-situ XPS experiments at 303 K (Figure 4a). The different distributions of m-CO_3^{2-} in Au/TiO_2 catalysts may be the reason for the different $Au^{\delta+}$ changing tendencies in Au/Ti-100 and Au/Ti-101 in XPS.

In addition, the desorption properties of carbonates were also studied. After CO absorption, the atmosphere was shifted to O_2. As can be seen in Figure 5b, d, and f, the carbonates will gradually desorb at different rates. We have integrated the absorption peaks of carbonates and plotted the carbonates' desorption curves as a function of time (Figure 6). Obviously, it

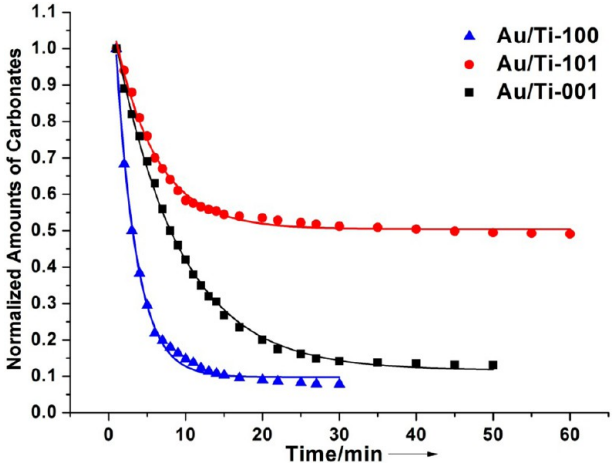

Figure 6. Normalized desorption curves of carbonates in O_2 atmosphere at 303 K on Au/TiO_2 catalysts with different TiO_2 crystal planes.

is more difficult to desorb carbonates on Au/Ti-101 than those on on Au/Ti-001 and Au/Ti-100, which is consistent with the strong interaction between Au NPs and carbonates in Au/Ti-101. Another interesting phenomenon can be observed in the desorption DRIFTS of Au/Ti-100. The peak at 1366 cm^{-1} shifts to 1384 cm^{-1}, indicating that a movement of m-CO_3^{2-} from TiO_2 support to Au/TiO_2 interface may have occurred. This movement of m-CO_3^{2-} should result in their decomposition at the Au/TiO_2 interface. In-situ DRIFTS experiments were also performed over Au/TiO_2 catalysts at 353 K; however, no signals corresponding to carbonates can be observed because of the thermal desorption (SI Figure S15). Because of the desorption of the carbonates, the $Au^{\delta+}$ in the Au/Ti-101 sample shows a variation tendency similar to that of Au/Ti-100 under O_2 and CO atmosphere at 353 K (as shown in Figure 4b). Thus, the ex-situ XPS and in situ DRIFTS results are consistent with the catalytic properties of Au/TiO_2.

On the basis of the above analysis and discussions, a schematic illustration to describe the crystal-plane effect on the catalytic properties of Au/TiO_2 is displayed in Figure 7. At low temperature (<320 K), the activation of O_2 on Au/TiO_2{100} plane interface is more favorable, resulting in the formation of $Au^{\delta+}$. When CO reacts with the active oxygen species, carbonates are formed on the TiO_2 support or Au/TiO_2 interface. The carbonates' desorption rates are also related to the crystal planes of TiO_2. As a consequence of the above processes, CO oxidation activities of Au/TiO_2 catalysts follow

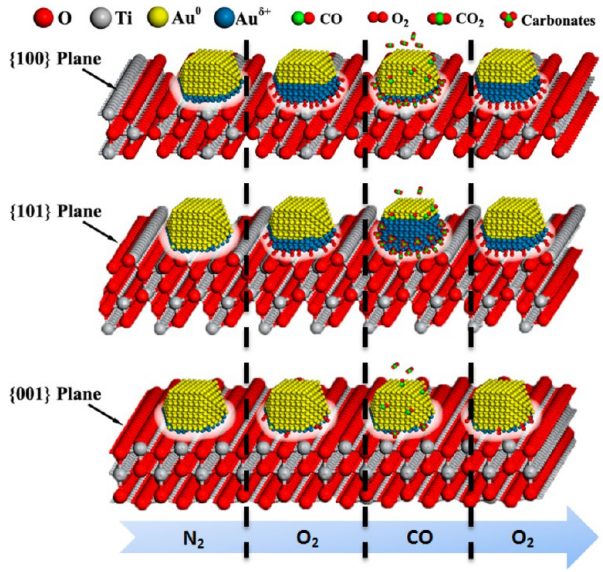

Figure 7. Schematic illustration of dynamic changes of Au NPs in Au/Ti-100 (top), Au/Ti-101 (middle), and Au/Ti-001 (lower) in different atmospheres at 303 K.

this order: Au/Ti-100 > Au/Ti-101 > Au/Ti-001. At higher temperature (>320 K), the CO oxidation mechanism is changed. The migration of active oxygen on different crystal planes may play a dominant role in the catalytic process of CO oxidation. On this point, {100} and {101} planes are more active than {001} planes, leading to higher activities of Au/Ti-101 and Au/Ti-100. Because of the different structures of the Au/TiO_2 interfaces, the activation of O_2 and formation, distribution, and desorption of carbonates are highly crystal-plane-dependent. Thus, the origins accounting for the different catalytic properties of the three Au/TiO_2 catalysts are the surface structures of the different TiO_2 crystal planes.

4. CONCLUSION

Through this work, we find that the crystal-plane effects on Au/TiO_2 catalysts are working through the interaction between the substrate molecules and the Au/TiO_2 interface. Combining the results obtained from ex-situ XPS and in situ DRIFTS, we can explain the different apparent activation energies at low temperature (<320 K) and high temperature (>320 K). However, the fundamental origins of the crystal-plane effects are still unrevealed at a molecular level. Maybe theoretical calculations will further provide some insights on this question.[47,48] Considering their different surface structures, we believe that tuning the crystal plane of the TiO_2 support will be an effective strategy to improve the catalytic performances of Au/TiO_2 catalysts.

■ ASSOCIATED CONTENT

Supporting Information

The preparation methods, characterizations, and some other related data. This material is available free of charge via the Internet at http://pubs.acs.org.

■ AUTHOR INFORMATION

Corresponding Authors

*Phone: +86 25 83592290. Fax: +86 25 83317761. E-mail: gaofei@nju.edu.cn.

*E-mail: donglin@nju.edu.cn

Notes

The authors declare no competing financial interest.

■ ACKNOWLEDGMENTS

Financial support from the National Nature Science Foundation of China (No. 21203091), the Natural Science Foundation of Jiangsu Province (BK2012298), the National 973 Program of China (No.2010CB732300), and the National Undergraduate Innovation Program (XZ101028426) are gratefully acknowledged.

■ REFERENCES

(1) Zhang, Y.; Cui, X.; Shi, F.; Deng, Y. *Chem. Rev.* **2012**, *112*, 2467−2505.
(2) Heitbaum, M.; Glorius, F.; Escher, I. *Angew. Chem., Int. Ed.* **2006**, *45*, 4732−4762.
(3) Somorjai, G. A.; Li, Y. *Introduction to Surface Chemistry and Catalysis*; John Wiley & Sons, Inc.: Hoboken, NJ, 2010.
(4) Goodman, D. W. *Catal. Lett.* **2005**, *99*, 1−4.
(5) Tauster, S. J. *Acc. Chem. Res.* **1987**, *20*, 389−394.
(6) Yang, L.; Shan, S.; Loukrakpam, R.; Petkov, V.; Ren, Y.; Wanjala, B. N.; Engelhard, M. H.; Luo, J.; Yin, J.; Chen, Y.; Zhong, C. J. *J. Am. Chem. Soc.* **2012**, *134*, 15048−15060.
(7) Ma, Z.; Dai, S. *Nano Res.* **2010**, *4*, 3−32.
(8) Shekhar, M.; Wang, J.; Lee, W. S.; Williams, W. D.; Kim, S. M.; Stach, E. A.; Miller, J. T.; Delgass, W. N.; Ribeiro, F. H. *J. Am. Chem. Soc.* **2012**, *134*, 4700−4708.
(9) Zhou, K.; Li, Y. *Angew. Chem., Int. Ed.* **2012**, *51*, 602−613.
(10) Zhou, K.; Wang, X.; Sun, X.; Peng, Q.; Li, Y. *J. Catal.* **2005**, *229*, 206−212.
(11) Long, R.; Mao, K.; Ye, X.; Yan, W.; Huang, Y.; Wang, J.; Fu, Y.; Wang, X.; Wu, X.; Xie, Y.; Xiong, Y. *J. Am. Chem. Soc.* **2013**, *135*, 3200−3207.
(12) Laursen, S.; Combita, D.; Hungria, A. B.; Boronat, M.; Corma, A. *Angew. Chem., Int. Ed.* **2012**, *51*, 4190−4193.
(13) Wang, Y.; Wang, F.; Song, Q.; Xin, Q.; Xu, S.; Xu, J. *J. Am. Chem. Soc.* **2013**, *135*, 1506−1515.
(14) Si, R.; Flytzani-Stephanopoulos, M. *Angew. Chem., Int. Ed.* **2008**, *47*, 2884−2887.
(15) Yi, G.; Yang, H.; Li, B.; Lin, H.; Tanaka, K.-i.; Yuan, Y. *Catal. Today* **2010**, *157*, 83−88.
(16) Fei, Z. Y.; Sun, B.; Zhao, L.; Ji, W. J.; Au, C. T. *Chem.—Eur. J.* **2013**, *19*, 6480−6487.
(17) Hu, L.; Peng, Q.; Li, Y. *ChemCatChem* **2011**, *3*, 868−874.
(18) Chen, M. S.; Goodman, D. W. *Science* **2004**, *306*, 252−255.
(19) Green, I. X.; Tang, W.; Neurock, M.; Yates, J. T., Jr. *Science* **2011**, *333*, 736−739.
(20) Haruta, M. *Chem. Rec.* **2003**, *3*, 75−87.
(21) Chen, M. S.; Goodman, D. W. *Catal. Today* **2006**, *111*, 22−33.
(22) Han, X.; Kuang, Q.; Jin, M.; Xie, Z.; Zheng, L. *J. Am. Chem. Soc.* **2009**, *131*, 3152−3153.
(23) Bond, G. C.; Thompson, D. T. *Catal. Rev.* **1999**, *41*, 319−388.
(24) Fujitani, T.; Nakamura, I. *Angew. Chem., Int. Ed.* **2011**, *50*, 10144−10147.
(25) Widemann, D.; Behm, R. J. *Angew. Chem., Int. Ed.* **2011**, *50*, 10241−10245.
(26) Li, Y. F.; Selloni, A. *J. Am. Chem. Soc.* **2013**, *135*, 9195−9199.
(27) (a) Tsukamoto, D.; Shiraishi, Y.; Sugano, Y.; Ichikawa, S.; Tanaka, S.; Hirai, T. *J. Am. Chem. Soc.* **2012**, *134*, 6309−6315. (b) Liu, H.; Kozlov, A. I.; Kozlova, A. P.; Shido, T.; Asakura, K.; Iwasawa, Y. *J. Catal.* **1999**, *185*, 252−264.
(28) Bond, G. C.; Thompson, D. T. *Gold Bull.* **2000**, *33*, 41−50.
(29) Barnard, A. S.; Zapol, P.; Curtiss, L. A. *Surf. Sci.* **2005**, *582*, 173−188.
(30) Erdem, B.; Hunsicker, R. A.; Simmons, G. W.; Sudol, E. D.; Dimonie, V. L.; El-Aasser, M. S. *Langmuir* **2001**, *17*, 2664−2669.
(31) Min, B. K.; Friend, C. M. *Chem. Rev.* **2007**, *107*, 2709−2724.
(32) Fu, Q.; Wagner, T. *Surf. Sci. Rep.* **2007**, *62*, 431−498.
(33) Fu, Q.; Saltsburg, H.; Flytzani-Stephanopoulos, M. *Science* **2003**, *301*, 935−938.
(34) Zhang, X.; Corma, A. *Angew. Chem., Int. Ed.* **2008**, *47*, 4358−4361.
(35) Herranz, T.; Deng, X.; Cabot, A.; Liu, Z.; Salmeron, M. *J. Catal.* **2011**, *283*, 119−123.
(36) Dumbuya, K.; Cabailh, G.; Lazzari, R.; Jupille, J.; Ringel, L.; Pistor, M.; Lytken, O.; Steinrück, H. P.; Gottfried, J. M. *Catal. Today* **2012**, *181*, 20−25.
(37) Fu, Q.; Yang, F.; Bao, X. *Acc. Chem. Res.* **2013**, DOI: 10.1021/ar300249b.
(38) Qi, L.; Tang, C.; Zhang, L.; Yao, X.; Cao, Y.; Liu, L.; Gao, F.; Dong, L.; Chen, Y. *Appl. Catal., B* **2012**, *127*, 234−245.
(39) Liao, L. F.; Lien, C. F.; Shieh, D. L.; Chen, M. T.; Lin, J. L. *J. Phys. Chem. B* **2002**, *106*, 11240−11245.
(40) Baltrusaitis, J.; Schuttlefield, J.; Zeitler, E.; Grassian, V. H. *Chem. Eng. J.* **2011**, *170*, 471−481.
(41) Liu, L.; Zhao, H.; Andino, J. M.; Li, Y. *ACS Catal.* **2012**, *2*, 1817−1828.
(42) Kim, H. Y.; Han, S. S.; Ryu, J. H.; Lee, H. M. *J. Phys. Chem. C* **2010**, *114*, 3156−3160.
(43) Su, H.-Y.; Yang, M.-M.; Bao, X.-H.; Li, W.-X. *J. Phys. Chem. C* **2008**, *112*, 17303−17310.
(44) Senanayake, S. D.; Stacchiola, D.; Liu, P.; Mullins, C. B.; Hrbek, J.; Rodriguez, J. A. *J. Phys. Chem. C* **2009**, *113*, 19536−19544.
(45) Daniells, S.; Overweg, A.; Makkee, M.; Moulijn, J. *J. Catal.* **2005**, *230*, 52−65.
(46) Parida, K. M.; Sahu, N.; Tripathi, A. K.; Kamble, V. S. *Environ. Sci. Technol.* **2010**, *44*, 4155−4160.
(47) Laursen, S.; Linic, S. *J. Phys. Chem. C* **2009**, *113*, 6689−6693.
(48) Liu, L. M.; McAllister, B.; Ye, H. Q.; Hu, P. *J. Am. Chem. Soc.* **2006**, *128*, 4017−4022.